APC^{FZR1} prevents nondisjunction in mouse oocytes by controlling meiotic spindle assembly timing

Janet E. Holt[a], Simon I. R. Lane[a], Phoebe Jennings[a], Irene García-Higuera[b], Sergio Moreno[b], and Keith T. Jones[a]

[a]School of Biomedical Sciences, University of Newcastle, Callaghan, NSW 2308, Australia; [b]Instituto de Biología Molecular y Celular del Cáncer, Centro de Investigación del Cáncer/Salamanca University, Campus Miguel de Unamuno, 37007 Salamanca, Spain

ABSTRACT **FZR1 is an anaphase-promoting complex (APC) activator best known for its role in the mitotic cell cycle at M-phase exit, in G1, and in maintaining genome integrity. Previous studies also established that it prevents meiotic resumption, equivalent to the G2/M transition. Here we report that mouse oocytes lacking FZR1 undergo passage through meiosis I that is accelerated by ~1 h, and this is due to an earlier onset of spindle assembly checkpoint (SAC) satisfaction and APC^{CDC20} activity. However, loss of FZR1 did not compromise SAC functionality; instead, earlier SAC satisfaction was achieved because the bipolar meiotic spindle was assembled more quickly in the absence of FZR1. This novel regulation of spindle assembly by FZR1 led to premature bivalent attachment to microtubules and loss of kinetochore-bound MAD2. Bivalents, however, were observed to congress poorly, leading to nondisjunction rates of 25%. We conclude that in mouse oocytes FZR1 controls the timing of assembly of the bipolar spindle and in so doing the timing of SAC satisfaction and APC^{CDC20} activity. This study implicates FZR1 as a major regulator of prometaphase whose activity helps to prevent chromosome nondisjunction.**

Monitoring Editor
Yixian Zheng
Carnegie Institution

Received: May 8, 2012
Revised: Jul 16, 2012
Accepted: Aug 14, 2012

INTRODUCTION

The first meiotic division is unique in leading to the separation of homologous chromosomes, and in mammalian oocytes it is a particularly protracted process lasting ~8–10 h. The luteinizing hormone surge preceding ovulation induces the fully-grown germinal vesicle (GV)–arrested oocyte to reenter the cell cycle by raising CDK1 activity to a level that permits nuclear envelope breakdown and chromatin condensation (Jones, 2008; Solc *et al.*, 2010). During subsequent progression through prometaphase, sister kinetochore pairs of homologous chromosomes (bivalents) attach to opposite poles of the assembling spindle. Similar to mitosis, the spindle assembly checkpoint (SAC) monitors the onset and fidelity of chromosome attachment to microtubules, inhibiting anaphase until the conditions of kinetochore occupancy and/or attachment are met (Brunet *et al.*, 2003; Wassmann *et al.*, 2003; Homer *et al.*, 2005a,b; McGuinness *et al.*, 2009; Hached *et al.*, 2011). Anaphase is subsequently driven by loss of SAC-mediated repression of the anaphase-promoting complex (APC), together with its coactivator CDC20. At this time APC^{CDC20} promotes the degradation of securin and cyclin B1, thus promoting cohesin cleavage by separase and lowering CDK1 activity, which permits chromosome segregation and polar body extrusion, respectively (Herbert *et al.*, 2003; Kudo *et al.*, 2006; Jones, 2008; Verlhac *et al.*, 2010).

Despite the presence of chromosome segregation machinery that is well conserved with respect to mitosis, bivalent separation in oocytes is inherently error prone, especially in women, resulting in embryonic aneuploidy (Hunt and Hassold, 2008; Jones and Lane, 2012). As such there is much interest in examining how prometaphase is regulated in mammalian oocytes. Pertinent to

This article was published online ahead of print in MBoC in Press (http://www.molbiolcell.org/cgi/doi/10.1091/mbc.E12-05-0352) on August 23, 2012.

Address correspondence to: Janet E. Holt (Janet.holt@newcastle.edu.au) and K.T.Jones@soton.ac.uk.

The authors declare no conflict of interest.

Abbreviations used: APC, anaphase-promoting complex; BUBR1, bub1-related kinase; CDC20, cell division cycle 20 homologue; CDK1, cyclin-dependent kinase 1; CENPC, centromere protein C; FZR1, Fizzy-Related 1; GAPDH, glyceraldehyde 3-phosphate dehydrogenase; GFP, green fluorescent protein; GV, germinal vesicle; GVB, germinal vesicle breakdown; H2B, histone 2B; HURP, hepatoma up-regulated protein; MII, meiosis II; MAD2, mitotic arrest deficient-like 2; NDJ, nondisjunction; PBE, polar body extrusion; PSSC, premature separation of sister chromatids; SAC, spindle assembly checkpoint; TPX2, targeting protein for *Xenopus* kinesin-like protein 2; ZP3, zona pellucida 3.

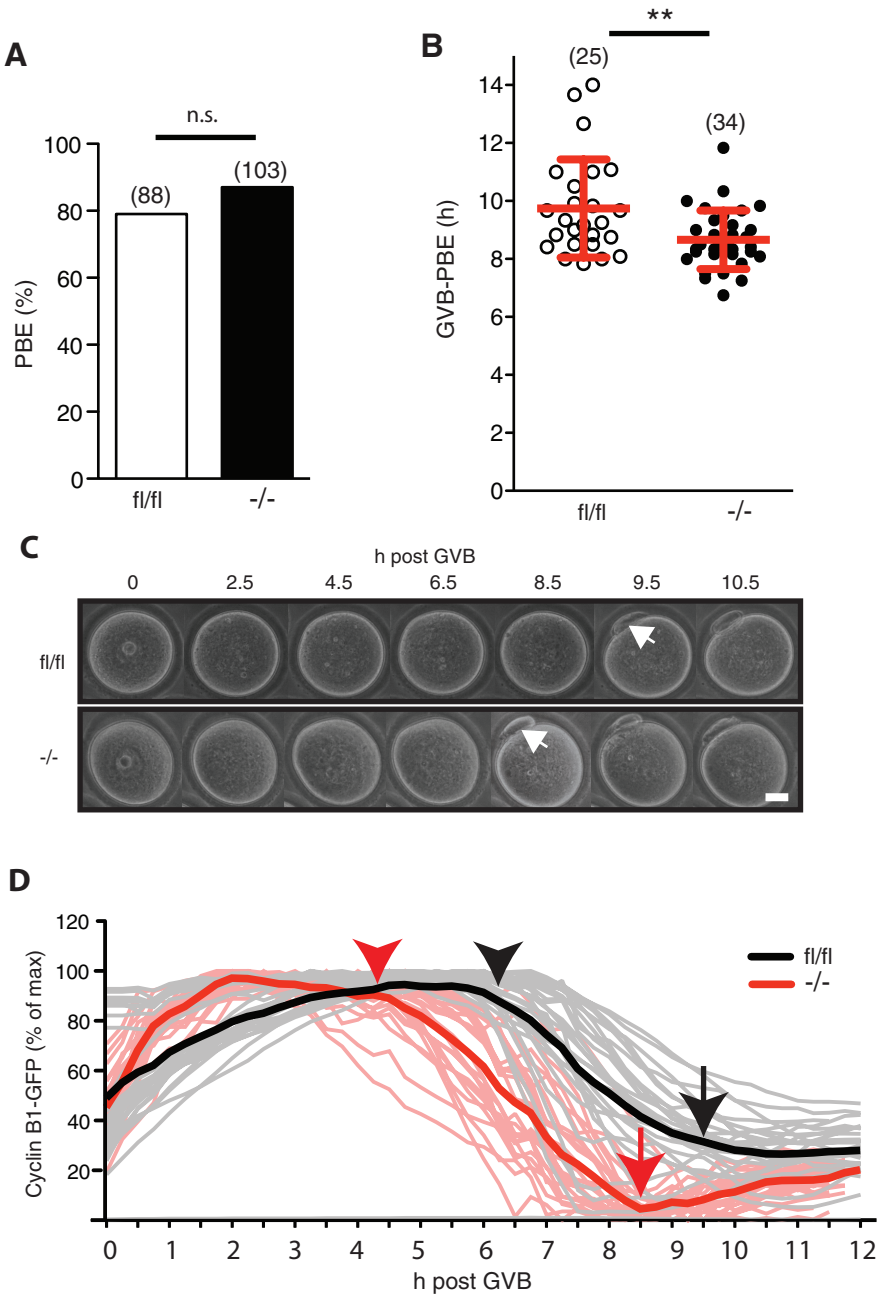

FIGURE 1: Accelerated passage through meiosis I in the absence of FZR1 is associated with earlier degradation of cyclin B1. (A) Polar body extrusion rates for fl/fl and *Fzr1*$^{-/-}$ oocytes matured in vitro (n.s., $p = 0.2$; χ^2). (B) Time between GVB and PBE for oocytes matured in vitro (**$p = 0.004$; *t* test) (C) Representative brightfield time-lapse images used to determine the GVB–PBE interval calculated in B. Arrows indicate the first appearance of PBE. (D) Cyclin B1-GFP degradation profile for fl/fl and *Fzr1*$^{-/-}$ oocytes ($n = 27$ and 24, respectively). Arrows indicate mean time of polar body extrusion for microinjected oocytes; arrowheads indicate onset of cyclin B1 degradation. In A and B, parentheses give numbers of oocytes analyzed; error bars in B show SD. Scale bar in C, 20 μm.

understanding this phenomenon, we and others have detected the activity of a second APC coactivator, Fizzy-Related 1 (FZR1), during both mammalian oocyte GV arrest and prometaphase I (Reis *et al.*, 2006, 2007; Marangos *et al.*, 2007; Yamamuro *et al.*, 2008; Homer *et al.*, 2009; Schindler and Schultz, 2009). Whereas high levels of CDK1 activity promote the affinity of CDC20 for the APC, the opposite is found for FZR1, such that APC^{FZR1} is the predominant form of the complex prior to metaphase when CDK1 activity is low (Zachariae *et al.*, 1998; Listovsky *et al.*, 2000; Reis *et al.*, 2007). APC^{FZR1} has a diverse and emerging range of substrates, and although best known for its role in regulating mitotic exit, has now been shown to play roles at other stages of the cell cycle (Qiao *et al.*, 2010; Wasch *et al.*, 2010).

Recently, using an oocyte-specific *Fzr1* mouse knockout, we showed that APC^{FZR1} is required to maintain GV arrest in fully grown oocytes in the ovary by keeping cyclin B1 levels low (Holt *et al.*, 2011). A role for APC^{FZR1} in prometaphase has also been suggested, with FZR1 shown to regulate levels of CDC20 and the SAC protein BUBR1 in oocytes (Reis *et al.*, 2007; Homer *et al.*, 2009). In somatic systems, disrupting negative regulators of FZR1, JNK, or Rae1-Nup98 complex that are known to be active around the time of prometaphase affects subsequent mitotic progression (Engelbert *et al.*, 2008; Gutierrez *et al.*, 2010). These data suggest that APC^{FZR1} may also be important during this period of the mitotic cell cycle.

A detailed analysis of the role of FZR1 function during meiosis I has been hampered by the need to use antisense knockdown approaches, and as such it has suffered from the disadvantages of incomplete knockdown and prolonged oocyte arrest in vitro. Here, therefore, we used an in vivo knockout model to examine FZR1 function during meiosis I in greater detail. Because a conventional FZR1 knockout is embryonic lethal (García-Higuera *et al.*, 2008; Li *et al.*, 2008), we developed an oocyte-specific knockout model of FZR1. Using ZP3 driven, Cre-recombinase–mediated loss of FZR1, we previously created mice with GV oocytes lacking FZR1 protein (Holt *et al.*, 2011). Despite an increased incidence of GVB in the ovary as a result of FZR1 loss (Holt *et al.*, 2011), we were able to obtain sufficient numbers of GV-arrested oocytes from these mice to allow examination of the process of meiosis I in its entirety. Here we describe a novel role for FZR1 in maintaining the proper timing of meiosis I by influencing spindle formation and thereby regulating the fidelity of chromosome segregation.

RESULTS

Accelerated meiosis I and earlier onset of cyclin B1 degradation associated with FZR1 loss

FZR1 was found not to be essential for completion of meiosis I. GV oocytes from control floxed mice (fl/fl) or *Fzr1*$^{-/-}$ knockouts underwent polar body extrusion (PBE) at the same rates after release into maturation medium (Figure 1A). However, passage through meiosis I was significantly accelerated in *Fzr1*$^{-/-}$ oocytes, with PBE occurring

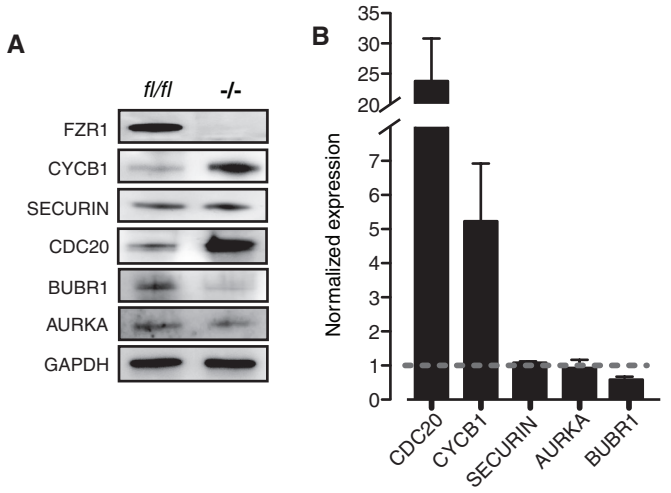

FIGURE 2: FZR1 regulates protein levels of CDC20, cyclin B1, and BUBR1. (A) Representative immunoblots of GV-arrested oocytes collected from *Fzr1*$^{-/-}$ mice or control littermates. At least three separate runs were performed, with $n = 50$ oocytes per lane. (B) Densitometric analysis of those immunoblots from A. Levels of the APC^{FZR1} substrates cyclin B1 and CDC20 were raised, whereas BUBR1 levels were less in *Fzr1*$^{-/-}$ oocytes. Error bars show SD.

at 8.7 h after GV breakdown (GVB), ~1 h earlier than for fl/fl oocytes (Figure 1, B and C).

The timing of meiosis I is controlled, in part, by APC^{CDC20}-mediated cyclin B1 degradation (Reis *et al.*, 2007; Jin *et al.*, 2010). Given that PBE was accelerated in *Fzr1*$^{-/-}$ oocytes, cyclin B1–green fluorescent protein (GFP) expression after cRNA injection was used to monitor for initiation of APC^{CDC20} activity. Levels sufficient for real-time imaging but having no perturbation on PBE timing were used (Hyslop *et al.*, 2004; Lane *et al.*, 2012). In fl/fl oocytes, cyclin B1 degradation began 6–7 h after GVB, but in *Fzr1*$^{-/-}$ oocytes this event began as early as 2 h after GVB, with substantial degradation by 4–5 h (Figure 1D). These observations were not an artifact associated with exogenous overexpression, since the same earlier onset of degradation was found in pooled groups of oocytes immunoblotted for endogenous cyclin B1 (Supplemental Figure S1). Therefore these data suggest that meiosis I length is shortened by loss of FZR1 as a result of earlier activation of the APC, resulting in the premature loss of cyclin B1.

Loss of FZR1 increases CDC20 and decreases BUBR1 in oocytes

The seemingly premature timing of APC^{CDC20} activity after FZR1 loss may have been caused by changes in levels of one or a number of proteins that are associated with this pathway. CDC20 is itself an APC^{FZR1} substrate (Pfleger and Kirschner, 2000; Zur and Brandeis, 2002; Reis *et al.*, 2006), and the stability of BUBR1, a component of the SAC, is reported to be dependent on the presence of FZR1 (Homer *et al.*, 2009). Indeed, consistent with these findings, we observed that CDC20 levels were nearly 25-fold higher and BUBR1 nearly 2-fold lower in *Fzr1*$^{-/-}$ oocytes (Figure 2, A and B). The very high levels of CDC20 and cyclin B1 suggest that both proteins are regulated in oocytes by APC^{FZR1} activity, but it is interesting that this is not the case for all potential substrates. Securin, which can be degraded by both APC^{CDC20} and APC^{FZR1}, and Aurora A, the levels of which are affected by FZR1 loss in some somatic cells (Peters, 2006; Floyd *et al.*, 2008; García-Higuera *et al.*, 2008), were both unchanged in oocytes in the absence of FZR1.

Activation of the SAC in *Fzr1*$^{-/-}$ oocytes using nocodazole

We believed that it was possible that after FZR1 loss the exceedingly high levels of CDC20 may act to neutralize the actions of the SAC. In addition, the lower levels of BUBR1 may compromise SAC function (Hwang *et al.*, 1998; Mondal *et al.*, 2007). Therefore, to examine for any potential decrease in functionality of the SAC, we challenged oocytes during maturation with the spindle poison nocodazole and assessed their ability to degrade cyclin B1-GFP and extrude polar bodies (Homer *et al.*, 2005b; Li *et al.*, 2009). A 100 nM dose of nocodazole prevented cyclin GFP degradation and blocked PBE in nearly all fl/fl and *Fzr1*$^{-/-}$ oocytes examined (Figure 3, A and B). A lower dose of nocodazole (50 nM), which blocked ~50% of fl/fl oocytes from undergoing PBE, also blocked PBE to a similar degree in *Fzr1*$^{-/-}$ oocytes (Figure 3B). In addition, we examined for the presence of the SAC protein MAD2 on the kinetochores. MAD2 is recruited to these sites in the absence of microtubule–kinetochore attachment and is therefore useful as a marker of kinetochore occupancy and so can be an indicator of SAC function (Wassmann *et al.*, 2003; De Antoni *et al.*, 2005; Gui and Homer, 2012; Lane *et al.*, 2012). MAD2 localized to kinetochores after nocodazole treatment in both fl/fl and *Fzr1*$^{-/-}$ oocytes (Figure 3C). These data therefore failed to uncover any significant defect in the SAC pathway in the absence of FZR1.

Lower levels of Mad2 on kinetochores after Fzr1 loss

Although the SAC appeared to be activated equally in *Fzr1*$^{-/-}$ and fl/fl oocytes to a nocodazole challenge, we wondered whether the time of initial SAC satisfaction might have been brought forward in those oocytes lacking FZR1. This earlier timing of SAC satisfaction would then be an explanation for the earlier onset of cyclin B1 degradation. Therefore we examined the time at which MAD2 protein began to leave the kinetochores of untreated in vitro matured oocytes. Levels of kinetochore-bound MAD2 were significantly lower in *Fzr1*$^{-/-}$ than in fl/fl oocytes at both 1.5 and 2.5 h post-GVB (Figure 4, A and B). Surprisingly, we also observed accumulation of MAD2 at sites consistent with both spindle poles, similar to that observed in controls at 5.5 h post GVB, a time when the SAC is normally satisfied and MAD2 has completely left the kinetochores (Figure 4A; Lane *et al.*, 2012). Therefore MAD2 begins to leave the kinetochores earlier in oocytes lacking FZR1 with a localization pattern that mimics controls at a later period of prometaphase.

Earlier spindle assembly in the absence of FZR1

The foregoing observations using nocodazole failed to uncover any obvious defect in the signaling pathway used by the SAC to silence the APC, and instead an earlier onset of SAC satisfaction appeared to underlie the accelerated passage through meiosis. Therefore we questioned whether the earlier loss of MAD2 from the kinetochores of *Fzr1*$^{-/-}$ oocytes was really as a consequence of an abrogated SAC. We were particularly intrigued by the earlier localization of Mad2 to the spindle poles of *Fzr1*$^{-/-}$ oocytes. Movement of Mad2 to spindle poles has previously been observed in mitosis and late prometaphase of oocyte meiosis I and is believed to occur in a dynein-dependent manner in response to the attachment of kinetochores to polar microtubules (Howell *et al.*, 2000; Zhang *et al.*, 2007). We therefore questioned whether meiotic spindle formation during prometaphase was altered in *Fzr1*$^{-/-}$ oocytes. We examined the dynamics of this process using tubulin immunostaining on fl/fl and *Fzr1*$^{-/-}$ oocytes between 1.5 and 4.5 h post GVB. At the earliest time point a microtubule ball was present in both control and *Fzr1*$^{-/-}$ oocytes, and no spindle poles were discernible (Figure 5A). Kinetochores were observed invariably to be

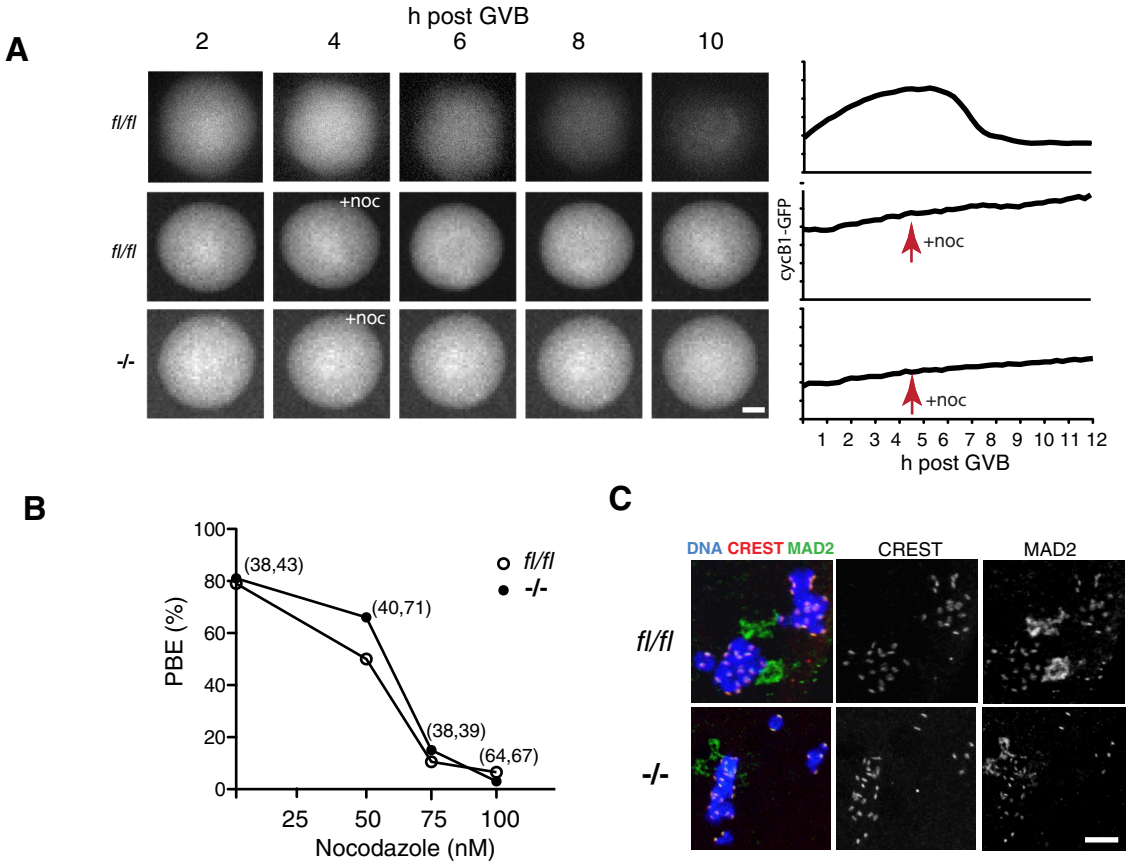

FIGURE 3: The microtubule poison nocodazole induces a robust SAC response in Fzr1$^{-/-}$ oocytes. (A) Cyclin B1-GFP expression and degradation profiles for fl/fl and *Fzr1*$^{-/-}$ oocytes in the absence or presence of nocodazole. Representative oocytes and traces are shown. Drug addition 4 h after GVB prevented cyclin B1 degradation in both fl/fl and *Fzr1*$^{-/-}$ oocytes. (B) Dose response of oocytes to nocodazole assessed by the ability of oocytes to undergo PBE within 12 h of GVB. A 100 nM dose of nocodazole blocked >95% of PBE in control fl/fl and *Fzr1*$^{-/-}$ oocytes (n.s., 50 nM, $p = 0.41$; 75 nM, $p = 0.77$; 100 nM, $p = 0.56$; χ^2). (C) MAD2 immunolocalization to kinetochores of fl/fl and *Fzr1*$^{-/-}$ oocytes after 100 nM nocodazole treatment 4 h post GVB. In B, parentheses give numbers of fl/fl and *Fzr1*$^{-/-}$ oocytes analyzed. Scale bar, (A) 20 μm, (B) 10 μm.

oriented toward the center of the microtubule ball, independent of FZR1, and this configuration was observed previously both in oocytes during meiosis I and in mitotic cells (Kitajima *et al.*, 2011; Magidson *et al.*, 2011). However, by 2.5 h a bipolar spindle had clearly been established in all *Fzr1*$^{-/-}$ oocytes but not in fl/fl controls, which were still spherical. Such differences in structure could be quantitated by measuring the spindle length taken as the longest measurement possible across the tubulin immunostaining (Figure 5B). Spindle length, pole to pole, was significantly greater in *Fzr1*$^{-/-}$ oocytes at 2.5 h compared with controls (Figure 5B). Control oocytes were delayed relative to *Fzr1*$^{-/-}$ by ~1 h, such that at 3.5 h the spindle length of control oocytes matched those of *Fzr1*$^{-/-}$ (Figure 5, A and B).

To confirm accelerated spindle formation by 2.5 h in *Fzr1*$^{-/-}$ oocytes, we also examined γ-tubulin localization as a marker of coalescing microtubule-organizing centers (Meng *et al.*, 2004; Dumont *et al.*, 2007). At 1.5 h post GVB, γ-tubulin was scattered among bivalents in both fl/fl and *Fzr1*$^{-/-}$ oocytes. However, by 2.5 h, in *Fzr1*$^{-/-}$ oocytes, γ-tubulin was localized predominantly in the regions developing into the spindle poles, in contrast to control oocytes, in which γ-tubulin still remained scattered (Figure 5C). Taken together, these observations suggest that meiosis I spindle formation is advanced in the absence of FZR1.

Earlier spindle assembly is independent of CDK1 activity, TPX2, or Eg5

APC^{FZR1} has potential substrates that have reported roles in mitotic and meiotic spindle assembly that could potentially lead to the premature assembly phenotype observed here. CDK1 regulates the activity of numerous spindle-associated proteins, including MAP4, Eg5, and tubulin itself (Ookata *et al.*, 1995; Fourest-Lieuvin *et al.*, 2006; Cahu *et al.*, 2008). We detected a 33% higher level of CDK1 activity in *Fzr1*$^{-/-}$ oocytes compared with fl/fl oocytes at 2.5 h after GVB (Figure 6A), which is consistent with the raised cyclin B1 levels in the absence of FZR1 (Figure 2 and Supplementary Figure S1). Therefore we next tested whether inhibition of CDK1 could rescue the premature spindle phenotype of *Fzr1*$^{-/-}$ oocytes. Treatment with a specific CDK1 inhibitor, flavopiridol (2.5 μM; Potapova *et al.*, 2006) during the 2.5 h after GVB reduced CDK1 activity to control levels but failed to affect the acceleration in spindle length observed in *Fzr1*$^{-/-}$ oocytes (Figure 6, A and B).

Two other potential candidates that may influence spindle assembly in the absence of FZR1 are TPX2 and HURP. TPX2 is a microtubule-associated protein responsible for Aurora kinase activation that has been implicated in spindle function and previously shown to be regulated by APC^{FZR1} in oocytes in vitro (Brunet *et al.*, 2008). Identified as an APC^{FZR1} substrate in somatic cells, HURP is required

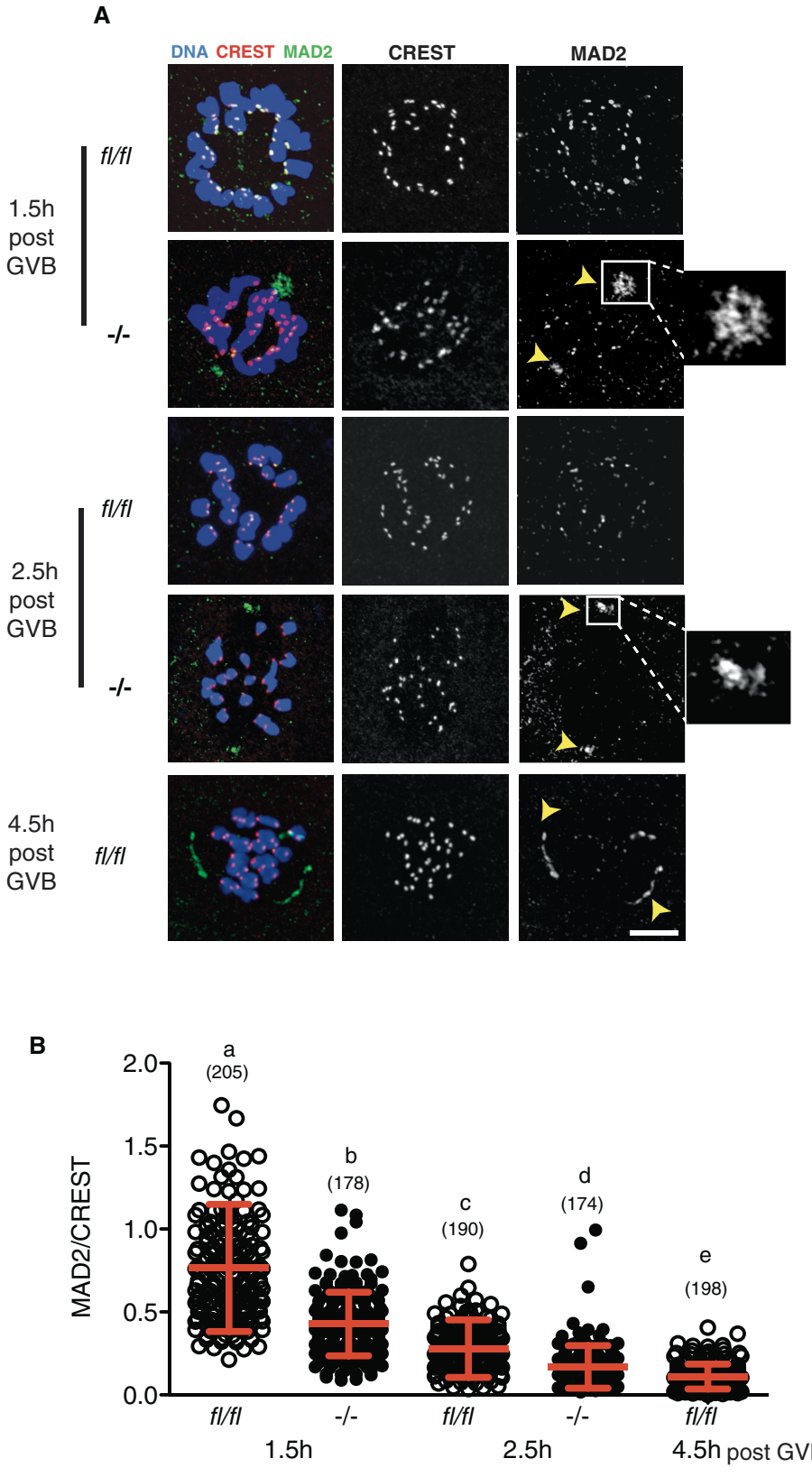

FIGURE 4: Earlier loss of MAD2 from kinetochores during prometaphase in *Fzr1*$^{-/-}$ oocytes. (A) Representative confocal *z*-stack images of MAD2/CREST immunostained in fl/fl and *Fzr1*$^{-/-}$ oocytes fixed during prometaphase. Arrowheads and insets indicate sites of intense MAD2 accumulation at predicted spindle poles for *Fzr1*$^{-/-}$ oocytes, similar to fl/fl oocytes at 4.5 h post GVB. (B) Kinetochore MAD2/CREST intensity ratios from at 1.5 and 2.5 h post GVB ($p < 0.001$; Kruskal–Wallis test with Dunn's post hoc test). Error bars (B) show SD; parentheses show numbers of kinetochores analyzed. Scale bar in A, 10 μm.

for the establishment and maintenance of spindle bipolarity in the oocyte (Breuer *et al.*, 2010; Song and Rape, 2010). However, we could not detect any increase in TPX2 or HURP protein levels in *Fzr1*$^{-/-}$ oocytes (Figure 6, C and D). Similarly, Eg5 is an important CDK1-regulated motor protein with a role in elongation of the mitotic and meiotic spindle and which possesses potential FZR1 degradation motifs (Cahu *et al.*, 2008; Fitzharris, 2009, 2012). We also did not detect any change in Eg5 levels or a band shift representative of Eg5 phosphorylation in *Fzr1*$^{-/-}$ oocytes (Figure 6, C and D). Therefore it remains possible that APC^{FZR1} regulates levels of an as-yet-unidentified spindle regulator that is responsible for maintaining proper timing of spindle formation.

MAD2 loss is associated with kinetochore stretch

To determine whether earlier formation of a microtubule spindle in the absence of FZR1 also leads to an earlier onset of microtubule–kinetochore interaction, we measured the stretch developing across bivalents. This stretch develops as a consequence of bivalent biorientation in response to stable kinetochore attachment to K-fibers and is measured as the distance apart of sister kinetochore pairs (Kitajima *et al.*, 2011; Nagaoka *et al.*, 2011; Lane *et al.*, 2012). At 1.5 and 2.5 h post GVB we measured the mean bivalent stretch and found that it was significantly greater in *Fzr1*$^{-/-}$ oocytes (Figure 7). Here we observed a small number of fully stretched bivalents as early as 1.5 h after GVB in *Fzr1*$^{-/-}$ oocytes, but no such bivalents were ever see at this time point in this biorientated state in control oocytes. At 2.5 h the mean bivalent stretch of *Fzr1*$^{-/-}$ oocytes was equivalent to that of control oocytes at 4.5 h, which shows that stretching of bivalents is advanced in the absence of FZR1 (Figure 7). Given that the onset of bivalent stretching was observed to occur at the same time as the MAD2 began to decrease on kinetochores, this supported the idea that the SAC is satisfied earlier in *Fzr1*$^{-/-}$ oocytes in response to stable kinetochore–microtubule attachment and associated tension on the bivalents.

Congression failure and nondisjunction of bivalents in *Fzr1*$^{-/-}$ oocytes

In *Fzr1*$^{-/-}$ oocytes the time between GVB and spindle elongation was shortened, and as such we predicted there may also be an effect on the ability of bivalents to congress onto a metaphase plate. This process occurs during prometaphase and is necessary for

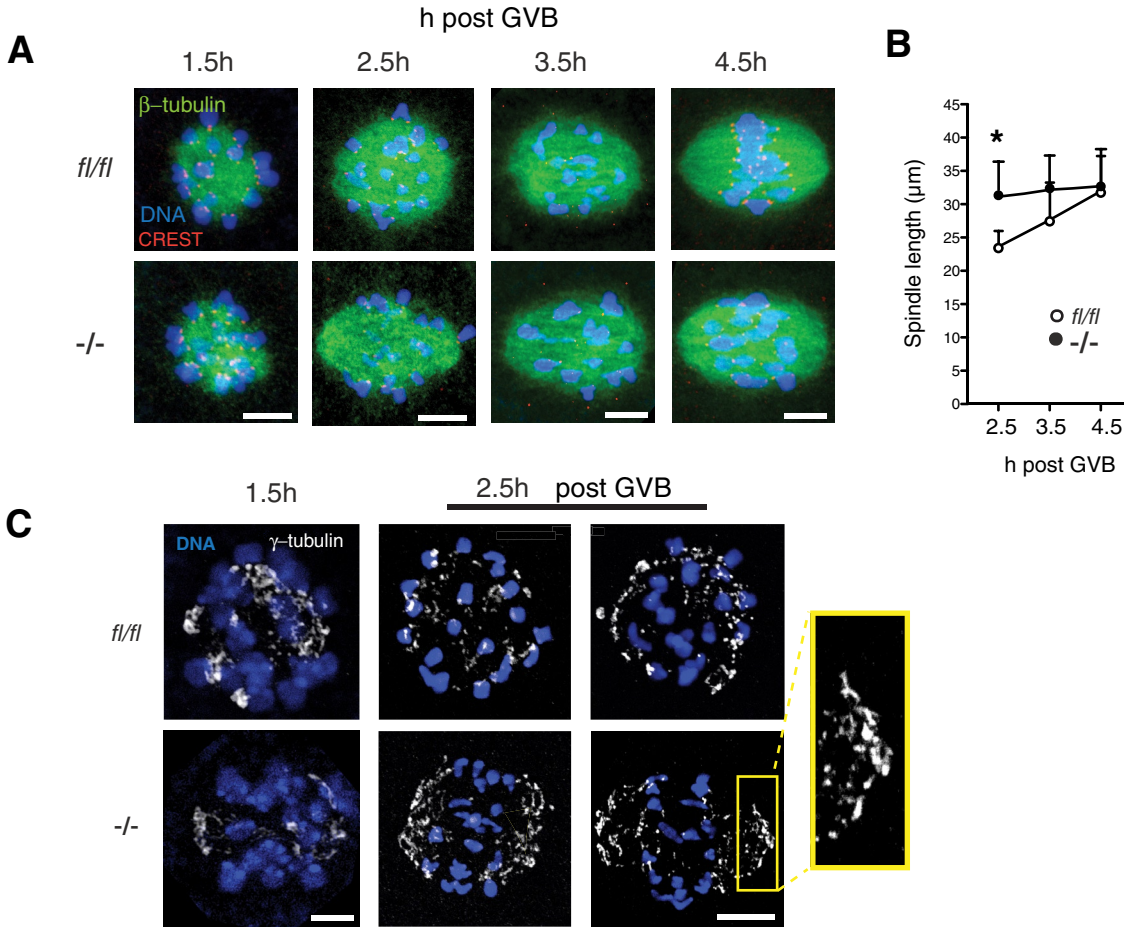

FIGURE 5: Accelerated meiosis I spindle elongation in *Fzr1*$^{-/-}$ oocytes. (A) Representative confocal *z*-stacks of meiosis I spindles in tubulin-immunostained oocytes at 1.5–4.5 h post GVB. Elongating bipolar spindles are present by 2.5 h in *Fzr1*$^{-/-}$ but not control fl/fl oocytes. (B) Spindle length measurements for *Fzr1*$^{-/-}$ and fl/fl oocytes fixed and immunostained at the indicated times post GVB (*$p = 0.012$; 3.5 h, $p = 0.16$; 4.5 h, $p = 0.8$; Students *t* test; $n = 5–7$ oocytes per time point). (C) γ-Tubulin–immunostained oocytes 1.5 and 2.5 h post GVB. Inset highlights accumulation of γ-tubulin at the developing spindle pole caps. Error bars in B indicate SD. Scale bars in A and C, 10 μm.

bivalent segregation during meiosis I (Dumont *et al.*, 2007; Kitajima *et al.*, 2011). Therefore we tracked bivalents during prometaphase using live-cell imaging by labeling chromosomes with histone2B-mCherry and kinetochores with CenpC. To examine congression, we analyzed the displacement of individual bivalents from the spindle equator over the period 1.5 to 4.5 h after GVB. In *Fzr1*$^{-/-}$ oocytes we observed a greater spread in displacement values compared with controls during this period, indicating a reduction in the ability of *Fzr1*$^{-/-}$ chromosomes to congress (Figure 8A). In the period immediately before anaphase, we observed that ~60% of *Fzr1*$^{-/-}$ oocytes (15 of 25) possessed one or more nonaligned bivalents located at some distance away from all the other bivalents on the metaphase plate (Figure 8, B–D). Some of these nonaligned bivalents were observed to return to the metaphase plate during the hour preceding anaphase; however, this was not the case in all oocytes (Figure 8D). In 24% of oocytes (6 of 25), nonaligned bivalents persisted until anaphase onset and as such were observed to undergo nondisjunction (Figure 8. D and E).

Finally, to confirm that reduced bivalent congression was associated with increased aneuploidy rates in *Fzr1*$^{-/-}$ oocytes, we analyzed oocytes after in vitro maturation using an in situ chromosome spreading technique (Figure 9A; Duncan *et al.*, 2009; Lane *et al.*, 2011). We observed a significant 3.5-fold rise in aneuploidy rates for *Fzr1*$^{-/-}$ oocytes, (Figure 9B) and noted that the rate of hypoploidy matched that of hyperploidy (Figure 9C). To determine whether true homologue nondisjunction or premature separation of sister chromatids (so called predivision) was the predominate aneuploidy type, we analyzed chromosome configurations (Figure 9, C and D). We confirmed that all but one of these eggs possessed sister chromatid pairs only and not separated sister chromatids (the remaining egg configuration could not be determined). Therefore, from a total of 12 aneuploid *Fzr1*$^{-/-}$ eggs that could be analyzed, 10 (representing 83%) had true nondisjunction as the predominant missegregation error.

DISCUSSION

Prometaphase in oocytes is a protracted and dynamic period during which correct attachment of bivalents to the meiotic spindle occurs in order to ensure the fidelity of chromosome segregation. Previous studies using antisense approaches implied a role for APC^{FZR1} at this time (Reis *et al.*, 2007; Homer *et al.*, 2009). Here we examined this period in molecular detail by using an oocyte-specific knockout model. We observed that FZR1 controlled the speed of spindle assembly in such a way that its loss accelerated bivalent biorientation and consequently the timing

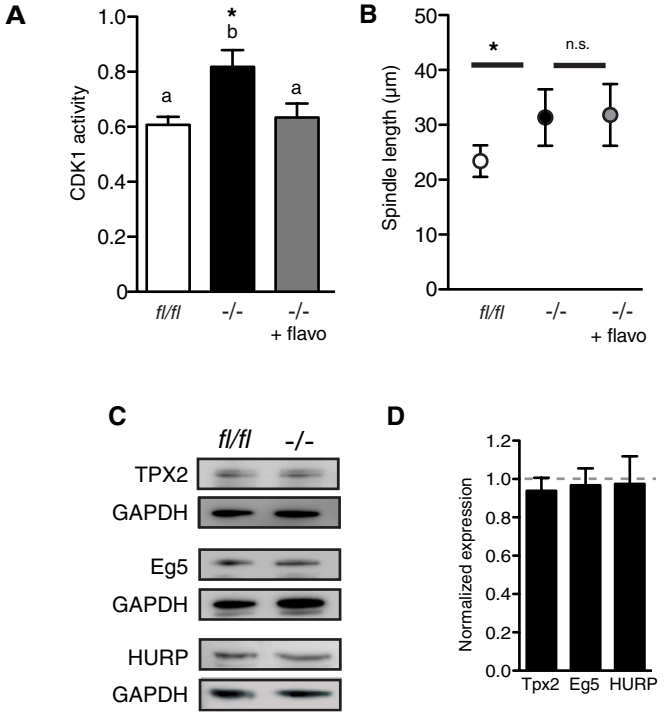

FIGURE 6: Premature spindle elongation is independent of CDK1 activity or TPX2, HURP, and Eg5 protein level in *Fzr1*$^{-/-}$ oocytes. (A) CDK1 activity measured using an enzyme-linked immunosorbent assay in *Fzr1*$^{-/-}$ and control fl/fl oocytes at 2.5 h after GVB. Activity levels were significantly higher in *Fzr1*$^{-/-}$ oocytes (*$p = 0.037$, one-way ANOVA with Tukey's test). Treatment with 2.5 μM flavopiridol reduced CDK1 activity to levels that were not significantly different from control oocytes. (B) Spindle length for control and *Fzr1*$^{-/-}$ oocytes, with and without flavopiridol treatment, measured 2.5 h after GVB. Flavopiridol treatment of *Fzr1*$^{-/-}$ oocytes did not significantly alter spindle length. (C) Representative immunoblots for TPX2, HURP, and Eg5 on protein from GV-arrested oocytes collected from *Fzr1*$^{-/-}$ mice or controls, with $n = 50$–100 oocytes per lane and at least two separate experiments performed. (D) Densitometric analysis of immunoblots in C. Error bars show SD.

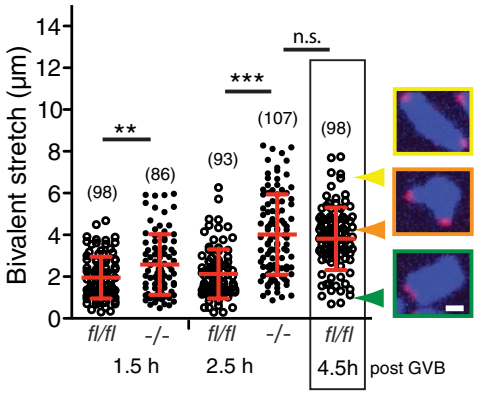

FIGURE 7: Earlier onset of bivalent stretching in the absence of FZR1. Bivalent stretch was measured as the distance between the pairs of sister kinetochores. Mean distances were increased for *Fzr1*$^{-/-}$ oocytes compared with fl/fl at 1.5 h and 2.5 h post GVB (**$p = 0.008$, ***$p < 0.001$; Mann–Whitney test). Images show representative homologue bivalent conformation types with corresponding distances. Error bars indicate SD; parentheses show the numbers of kinetochores analyzed. Scale bar, 2 μm.

of SAC satisfaction. This meiotic acceleration was detrimental to the fidelity of bivalent segregation, leading to high rates of homologue nondisjunction. Rather surprisingly, therefore, we uncovered a meiotic role of FZR1 in the timing of spindle assembly and the prevention of aneuploidy.

Loss of FZR1 leads to earlier onset of APC^{Cdc20} activity but does not compromise SAC function

Loss of FZR1 accelerated the time from GVB to PBE, a result consistent with data obtained using antisense morpholino knockdown (Reis *et al.*, 2007). We interpret this accelerated PBE in both models as confirming that FZR1 loss has an impact on meiosis I progression during only the very latest stages of follicular maturation and/or during prometaphase. This is because the impact on meiosis was no greater in our knockout model, in which FZR1 is lost only after follicular recruitment into the growing pool (Holt *et al.*, 2011).

The premature onset of cyclin B1 degradation in the absence of FZR1 was caused by earlier activation of APC^{CDC20}. Therefore our initial hypothesis was that loss of FZR1 led to an accelerated passage through meiosis I and generated higher rates of aneuploidy because the SAC was being bypassed. This idea was supported by changes in the levels of two proteins that together may have conspired to weaken the ability of the SAC to function—first, higher levels of CDC20, the most downstream target of the SAC and coactivator of the APC, needed to induce cyclin B1 degradation; and second, reduced amounts of the SAC component BUBR1, which, although not a substrate of the APC, requires FZR1 for its stability (Homer *et al.*, 2009). In addition to these protein changes, we also observed that in FZR1-knockout oocytes MAD2 began to leave kinetochores earlier, suggesting a satisfaction of the SAC at a premature time point compared with controls. Given all of these predictors of a compromised SAC function in FZR1 knockout oocytes, it was therefore disappointing for our initial hypothesis that we could produce a very good SAC-imposed inhibition of the APC and meiotic arrest in the absence of FZR1 after nocodazole addition. In fact the response of FZR1-knockout oocytes to this spindle poison was identical to that of control oocytes in terms of sensitivity to nocodazole dose, recruitment of MAD2 onto kinetochores, and inhibition of cyclin B1 degradation. In summary, therefore, we were left with conflicting observations of a much earlier SAC satisfaction after FZR1 loss, as measured by premature dissociation of at least some MAD2 from kinetochores and earlier cyclin B1 degradation, but nonetheless a normal, robust SAC response to nocodazole that was indistinguishable from that in controls. Such findings prompted us to speculate on an alternative hypothesis for the earlier activation of APC^{Cdc20}. This was that the conditions satisfying the SAC were being met at a much earlier time point in FZR1-knockout oocytes.

The meiotic spindle forms more quickly in the absence of FZR1

Associated with the earlier dissociation of MAD2 from kinetochores in FZR1-knockout oocytes was the appearance of bivalent stretching. This stretch develops as a result of stable kinetochore–microtubule interaction and biorientation, thus generating tension across the bivalent, and has been used as a marker of these processes in a number of oocyte studies (Kitajima *et al.*, 2011; Nagaoka *et al.*, 2011; Lane *et al.*, 2012). This stretch was generated as a result of

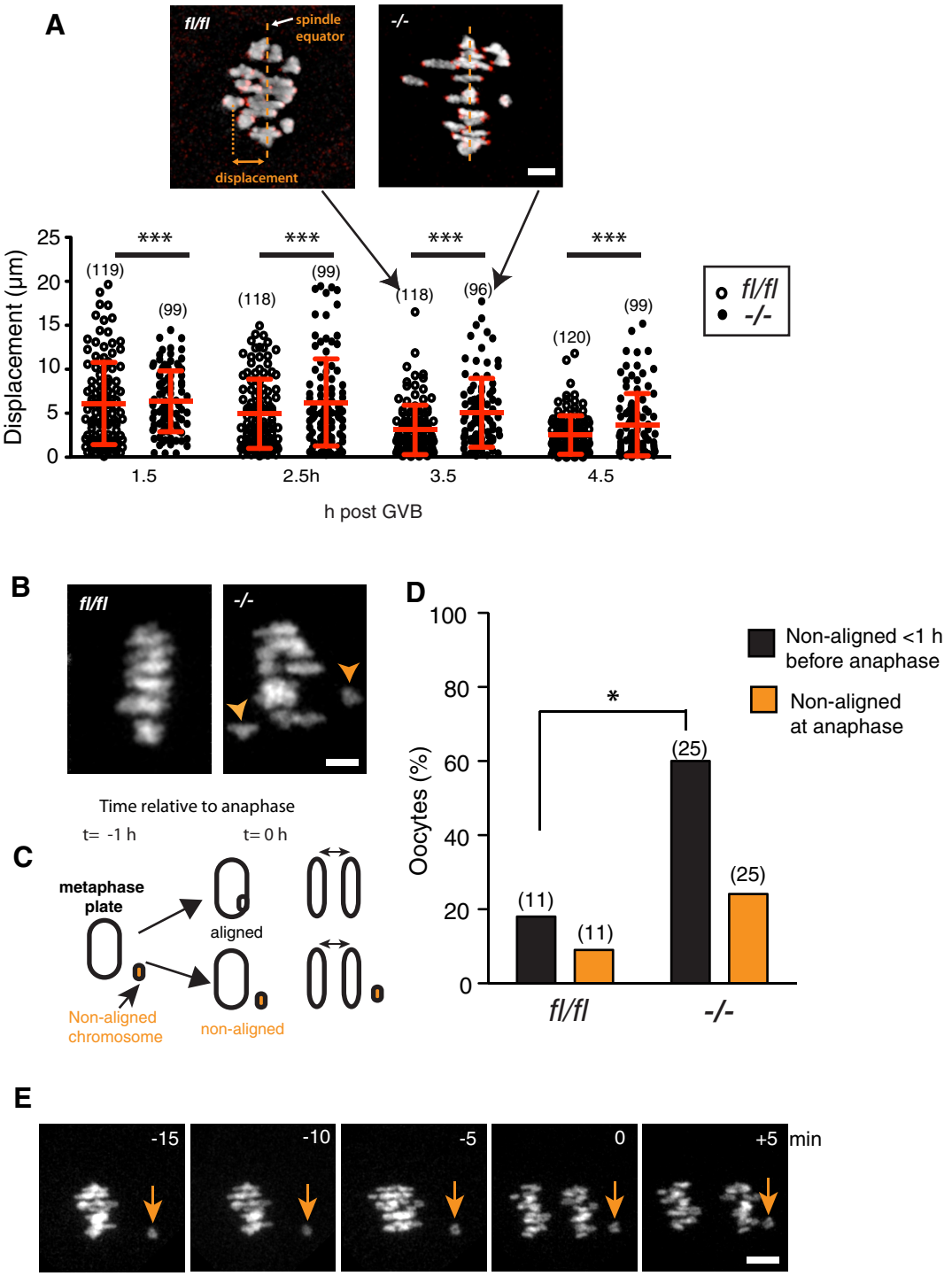

FIGURE 8: Congression and metaphase alignment failure in *Fzr1*$^{-/-}$ oocytes. (A) Displacement values for *Fzr1*$^{-/-}$ and fl/fl bivalents from the spindle equator during prometaphase. The spread of displacement values was greater for *Fzr1*$^{-/-}$ oocytes at all time points measured, indicating poor congression of bivalents compared with controls (***$p < 0.001$; Levene's test for variance). Representative confocal *z*-stack images of fl/fl and *Fzr1*$^{-/-}$ H2BmCherry/CENPC-labeled chromosomes at 3.5 h after GVB are shown. Error bars indicate SD, and the line indicates the mean. Parentheses indicate the numbers of bivalents examined from a total of five to six oocytes per group. (B) Representative confocal *z*-stack images of fl/fl and *Fzr1*$^{-/-}$ H2BmCherry-labeled chromosomes 1 h before anaphase I, showing failure of congression in the *Fzr1*$^{-/-}$ oocyte. Arrowheads indicate nonaligned bivalents. (C) Schematic showing fate of nonaligned bivalents in the 1 h before anaphase. Nonaligned bivalents either returned to the metaphase plate or remained separate and were consequently nonaligned at anaphase onset. (D) Percentage of fl/fl and *Fzr1*$^{-/-}$ oocytes with nonaligned bivalents 1 h before anaphase and at the onset of anaphase (*$p = 0.03$; Fisher's exact test). (E) Representative time series of *Fzr1*$^{-/-}$ bivalents in the minutes preceding anaphase I. Arrows indicate a nonaligned bivalent that fails to return to the metaphase plate before anaphase onset. Parentheses in C indicate the numbers of eggs analyzed. Scale bars, (A) 5 µm, (D) 15 µm.

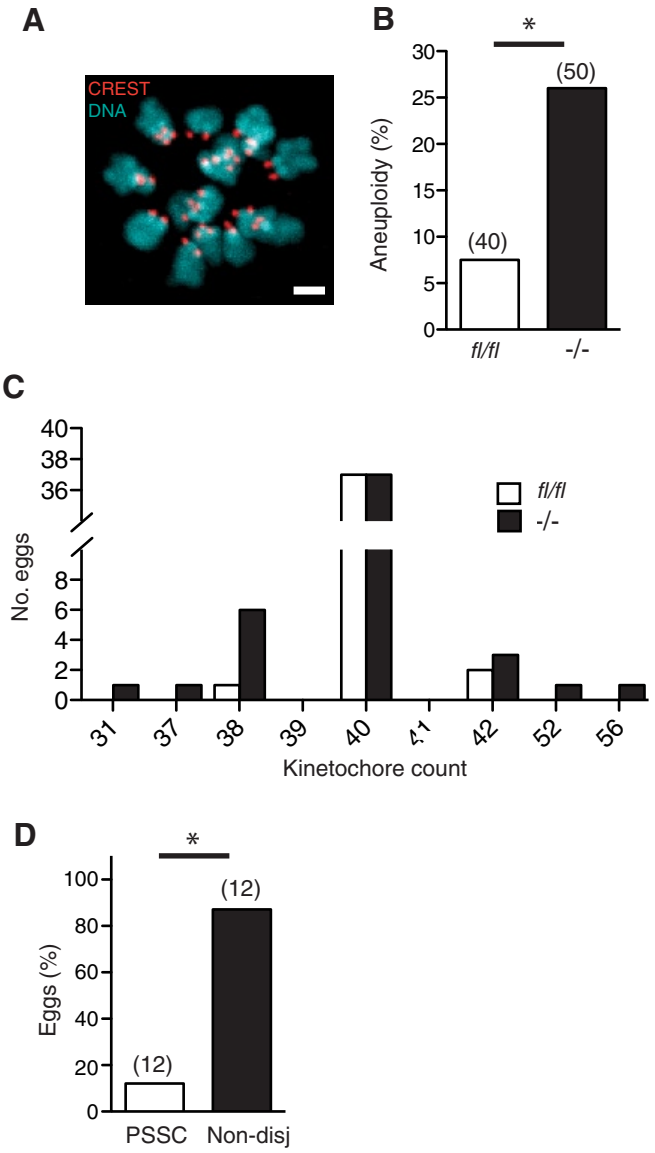

FIGURE 9: Increased rates of homologue nondisjunction in *Fzr1*$^{-/-}$ oocytes. (A) Representative confocal image of a monastrol-induced spread from a meiosis II (MII) egg used for aneuploidy analysis. (B) Aneuploidy rates in fl/fl and *Fzr1*$^{-/-}$ oocytes *matured in vitro*. *$p = 0.045$; χ^2. (C) Kinetochore counts from individual eggs scored in B. Rates of hyperploidy matched rates of hypoploidy in *Fzr1*$^{-/-}$ eggs (n.s., $p = 0.41$; χ^2). (D) Nondisjunction prevailed over PSSC in aneuploid *Fzr1*$^{-/-}$ eggs (*$p = 0.02$; χ^2). Parentheses in B and D indicate numbers of eggs analyzed. Scale bar in A, 2 μm.

much quicker bipolar spindle assembly in oocytes lacking FZR1—as early as 2.5 h after GVB, and some 1 h ahead of controls. The spindles that formed under these conditions appeared no different from controls by 3.5–4.5 h after GVB, suggesting that spindle formation was not grossly dysfunctional, merely accelerated. Thus, for example, independent of FZR1, the accumulation of MAD2 at the spindle poles was an event associated with SAC satisfaction, as it is in mitotic cells (Howell *et al.*, 2000).

We examined some obvious reasons for the accelerated onset of spindle assembly after FZR1 loss. Despite the higher prometaphase CDK1, a reduction of this kinase activity to control levels failed to restore the normal timing of this process. Alternative explanations were also examined with respect to proteins that may affect spindle assembly timing. For example, although previous reports demonstrated that APC^{FZR1} mediates TPX2 and HURP degradation (Brunet *et al.*, 2008; García-Higuera *et al.*, 2008; Song and Rape, 2010) and that Eg5 possesses potential KEN degradation boxes, we failed to detect a change in any of these proteins. Their failure to accumulate in *Fzr1*$^{-/-}$ oocytes is also shared by two other known FZR1 substrates that we examined, Aurora A and securin (Figure 2), suggesting that the resting levels of some FZR1 substrates are likely determined by other factors, such as their rate of synthesis, rather than their rate of degradation. Therefore it remains to be determined which protein(s) may be the direct or indirect targets of APC^{FZR1} regulating the timing of spindle elongation.

Dependence of chromosome congression on the timing of spindle formation

We observed failed bivalent congression in the majority of oocytes lacking FZR1, and this resulted in a higher incidence of nonalignment at anaphase onset. This matched the rate of nondisjunction, suggesting that the fate of most of these bivalents during division was to cosegregate.

Nonaligned bivalents located between the spindle pole and the metaphase plate are likely to be positioned there as a result of incorrect or failed attachment of the two pairs of sister kinetochores within a bivalent—for example, when both pairs of sisters are attached to the same pole. Recent detailed analysis of chromosome and kinetochore tracking revealed that congression of bivalents involves multiple rounds of kinetochore–microtubule error attachment–correction, and this phase precedes spindle elongation (Kitajima *et al.*, 2011). On the basis of our observations of events during meiosis I in the absence of FZR1, we propose that premature spindle elongation shortens the time period available for chromosome congression and correction of kinetochore attachment errors, ultimately resulting in a higher incidence of aneuploidy. The fact that small numbers of nonaligned bivalents do not trigger the SAC and impose arrest is not surprising, given that the SAC in mouse oocytes appears primarily to respond to lack of microtubule attachment to kinetochores rather than incorrect attachment or chromosome position (Gui and Homer, 2012; Kolano *et al.*, 2012; Lane *et al.*, 2012).

Analysis of chromosomal aneuploidies in human and mouse eggs show that both homologue nondisjunction (NDJ) and premature separation of sister chromatids (PSSC) contribute to aneuploidy (Kuliev *et al.*, 2011; Merriman *et al.*, 2012). Of interest, in our model we only observed NDJ rather than PSSC. The latter appears in many studies to be the underlying type of aneuploidy associated with advanced maternal age and may be explained by the gradual loss of the proteins associated with chromosome cohesion over the months, years, or decades of GV arrest (Chiang *et al.*, 2010; Lister *et al.*, 2010). Similarly, mitotic models in which SAC proteins are absent or greatly disrupted also result in PSSC (Michel *et al.*, 2001; Perera *et al.*, 2007). In these scenarios, PSSC is believed to be the result of SAC failure to detect incorrect microtubule attachment, leading to missegregation of sister chromatids. Taken together, this evidence supports the idea that aneuploidy in the absence of FZR1 is a not a result of disruption of chromosome cohesion or severe loss of SAC fidelity. Instead, it is the failure of bivalents to congress and so align on the metaphase plate that results in these homologues undergoing NDJ at anaphase onset. This is aided by the finding that the SAC in mouse oocytes fails to detect such alignment defects (Gui and Homer, 2012; Lane *et al.*, 2012).

In conclusion, we uncovered a role for the APC coactivator FZR1 in regulating the timing of spindle assembly in meiosis I. This appears to be novel and is not related to any up-regulation in CDK1 activity. Given that mammalian homologue segregation is inherently error prone, the present study brings us a step closer to unraveling the reasons behind this phenomenon. Further investigations may reveal whether this function of FZR1 also translates to the mitotic cell cycle.

MATERIALS AND METHODS

Materials

All materials were from Sigma-Aldrich (Castle Hill, Australia) unless otherwise specified.

Generation of oocyte-targeted *Fzr1*-knockout mice

Fzr1$^{fl/fl}$ mice were generated as previously described (García-Higuera *et al.*, 2008). Female *Fzr1*$^{fl/fl}$ mice were mated with ZP3Cre[C57BL/6-Tg(Zp3-cre)93Knw] males. F1 male offspring with the genotype Fzr$^{+/fl}$/ZP3Cre+ were mated with *Fzr1*$^{fl/fl}$ females to create oocyte-specific *Fzr1* knockout (*Fzr1*$^{-/-}$) and control *Fzr1*$^{fl/fl}$ (fl/fl) littermates (Holt *et al.*, 2011). Genotyping of mice was performed as described previously (García-Higuera *et al.*, 2008; Holt *et al.*, 2011).

Gamete collection and culture

All mice were used in accordance with ethics procedures approved by the University of Newcastle, Australia. Oocytes from fully grown follicles were collected from 4- to 6-wk old mice killed by cervical dislocation as previously described (Holt *et al.*, 2011). M2 media was used for bench handling, microinjection, and maturation. MEM media was used for long-term culture where imaging was not required. Milrinone (10 µM) was used to maintain GV arrest.

Microinjections and live-cell imaging

cRNA was made using a modified pRN3 vector. GFP-tagged cyclin B1 or H2B mCherry and CENP-C GFP-capped RNA was synthesized using T3 mMESSAGE mMACHINE (Life Technologies, Carlsbad, CA) and dissolved in nuclease-free water to a concentration of 1 µg/µl before use. Microinjections were made on the heated stage of a Nikon TE300 inverted microscope (Nikon, Sydney, Australia) in M2 media as previously described (Holt *et al.*, 2011; Lane *et al.*, 2012). Brightfield and epifluorescence images were captured using a Nikon Biostation IM or a Princeton Interline MicroMax charge-coupled device camera (Roper Scientific, Trenton, NJ) and data recorded using MetaMorph and MetaFluor software (Molecular Devices, Sunnyvale, CA).

Immunofluorescence

For aneuploidy analysis, oocytes were pretreated for 2 h in 200 µM monastrol at 37°C. Oocytes were fixed and permeabilized in 2% formaldehyde in PHEM buffer (60 mM 1,4-piperazinediethanesulfonic acid, 25 mM 4-(2-hydroxyethyl)-1-piperazineethanesulfonic acid, 25 mM ethylene glycol tetraacetic acid, 4 mM $MgSO_4$) with 0.1% Triton X-100 and 1 µM Taxol. Blocking was performed in 7% normal goat serum in phosphate-buffered saline (PBS) with 0.1% Tween. Primary antibodies were diluted in PBS with 1% bovine serum albumin/0.1% Tween with overnight incubation at 4°C. Tubulin (A11126) was from Invitrogen/Life Technologies Australia (Victoria, Australia) and CREST (90C1058) from Cortex Biochem (San Leandro, CA); MAD2 was a gift of R. H. Chen (Taiwan). Secondary antibodies were Alexa 488, 555, and 633 conjugated (Invitrogen). Oocytes were counterstained with Hoechst 33258 (20 µg/ml) before mounting in Citifluor (Citifluor, London, United Kingdom).

Confocal microscopy

Images were acquired using an Olympus FV1000 (Olympus, Tokyo, Japan) equipped with a 60×/1.2 numerical aperture UPLSAPO oil immersion objective and housed in a 37°C temperature-controlled environment. *Z*-series were captured at 0.5-µm intervals. Data analysis was performed using FluoView Software FV10-ASW2.0 (Olympus) and ImageJ (National Institutes of Health, Bethesda, MD) using macros designed in-house. Mad2/CREST ratios were calculated from colocalized signals after background subtraction as described in Lane *et al*. (2012). To improve the CENPC kinetochore signals, images were processed using ImageJ software by the subtraction of a 10-pixel Gaussian blur from a 2-pixel Gaussian blur. The positions of the kinetochores for each bivalent were logged using semiautomated ImageJ macros. Algorithms then trialed 1 million spindle orientations to establish the best fit with the bivalent kinetochore position in three dimensions. A second best-fit algorithm then fixed the position of the spindle equator, from which the displacement for each bivalent was determined for each time point.

Immunoblotting

Oocytes were lysed in reducing SDS buffer and proteins separated on a NuPage 4–12% gel as previously described (Holt *et al.*, 2011). Immunoblotting was performed using antibodies for FZR1 (ab3242; Abcam, Cambridge, United Kingdom), gylceraldehyde-3-phosphate dehydrogenase (G9545; Sigma-Aldrich), Aurora A kinase (ab13824; Abcam), cyclin B1 (ab72; Abcam), securin (ab3305; Abcam), CDC20 (sc8358; Santa Cruz Biotechnology, Santa Cruz, CA), TPX2 (ab32795; Abcam), Hurp (sc98809; Santa Cruz Biotechnology), Eg5 (NB100-8467; Novus Biologicals, Littleton, CO), γ-tubulin (T6557; Sigma-Aldrich), and secondary immunoglobulin horseradish peroxidase (Dako, Glostrup, Denmark). Secondary incubation was followed by use of ECL Detection reagents (GE Healthcare Australia, Rydalmere, Australia) according to the manufacturer's instructions.

CDK1 kinase assays

The CDK1 enzyme-linked immunosorbent assay was performed using a Mesacup cdc2 kinase assay kit as per the manufacturer's instructions (5234; MBL, Nagoya, Japan). Oocytes to be assayed were treated for 1 h with 2.5 µM flavopiridol in media also containing milrinone to maintain meiotic arrest. Oocytes were then washed into media containing flavopiridol alone and collected for assay at 2.5 h post GVB. Ten oocytes per sample were washed three times in PBS/polyvinylpyrrolidone before lysis in 5 µl of nondenaturing cell lysis buffer (9803; Cell Signaling Technologies, Beverly, MA) containing 1 mM phenylmethylsulfonyl fluoride and frozen at –80°C until use. Lysate was added to 45 µl of Mesacup cdc2 kinase buffer containing biotinylated mouse vimentin (MV) peptide and ATP. Detection of MV peptide phosphorylation was performed by incubating the reaction product on microwell strips coated with anti–phospho-MV peptide monoclonal antibody, followed by incubation with streptavidin-conjugated peroxidase. Absorbance of peroxidase substrate was read at 492 nm and expressed as optical density.

Statistical analysis

Statistical analysis was performed using Prism, version 5 (GraphPad Software, La Jolla, CA). Means analysis was performed using an unpaired Student's *t* test, Mann–Whitney test, analysis of variance (ANOVA) with a Tukey's post hoc test, or Kruskal–Wallis test with Dunn's post hoc test. Dichotomous data were analyzed by a chi-squared test with Yates correction. Variance was calculated using Levene's test.

ACKNOWLEDGMENTS

We gratefully acknowledge the technical assistance of J. L. Weaver, K. Minahan, Y. Yun, and S. M. T. Tran. We thank E. A. McLaughlin for assistance with development of the ZP3CreFZRlox transgenic mouse line, R. H. Chen for the gift of the Mad2 antibody, and Y. Watanabe for the CENP C construct. This work was funded by a grant from the Australia Research Council (DP1101100418) to K.T.J. and S.M. J.E.H. is an Australian Research Council Discovery Early Career Researcher Award Fellow.

REFERENCES

Breuer M, Kolano A, Kwon M, Li CC, Tsai T, Pellman D, Brunet S, Verlhac MH (2010). HURP permits MTOC sorting for robust meiotic spindle bipolarity, similar to extra centrosome clustering in cancer cells. J Cell Biol 191, 1251–1260.

Brunet S, Dumont J, Lee KW, Kinoshita K, Hikal P, Gruss OJ, Maro B, Verlhac MH (2008). Meiotic regulation of TPX2 protein levels governs cell cycle progression in mouse oocytes. PloS One 3, e3338.

Brunet S, Pahlavan G, Taylor S, Maro B (2003). Functionality of the spindle checkpoint during the first meiotic division of mammalian oocytes. Reproduction 126, 443–450.

Cahu J, Olichon A, Hentrich C, Schek H, Drinjakovic J, Zhang C, Doherty-Kirby A, Lajoie G, Surrey T (2008). Phosphorylation by Cdk1 increases the binding of Eg5 to microtubules in vitro and in *Xenopus* egg extract spindles. PloS One 3, e3936.

Chiang T, Duncan FE, Schindler K, Schultz RM, Lampson MA (2010). Evidence that weakened centromere cohesion is a leading cause of age-related aneuploidy in oocytes. Curr Biol 20, 1522–1528.

De Antoni A *et al*. (2005). The Mad1/Mad2 complex as a template for Mad2 activation in the spindle assembly checkpoint. Curr Biol 15, 214–225.

Dumont J, Petri S, Pellegrin F, Terret ME, Bohnsack MT, Rassinier P, Georget V, Kalab P, Gruss OJ, Verlhac MH (2007). A centriole- and RanGTP-independent spindle assembly pathway in meiosis I of vertebrate oocytes. J Cell Biol 176, 295–305.

Duncan FE, Chiang T, Schultz RM, Lampson MA (2009). Evidence that a defective spindle assembly checkpoint is not the primary cause of maternal age-associated aneuploidy in mouse eggs. Biol Reprod 81, 768–776.

Engelbert D, Schnerch D, Baumgarten A, Wasch R (2008). The ubiquitin ligase APC(Cdh1) is required to maintain genome integrity in primary human cells. Oncogene 27, 907–917.

Fitzharris G (2009). A shift from kinesin 5-dependent metaphase spindle function during preimplantation development in mouse. Development 136, 2111–2119.

Fitzharris G (2012). Anaphase B precedes anaphase a in the mouse egg. Curr Biol 22, 437–444.

Floyd S, Pines J, Lindon C (2008). APC/C Cdh1 targets aurora kinase to control reorganization of the mitotic spindle at anaphase. Curr Biol 18, 1649–1658.

Fourest-Lieuvin A, Peris L, Gache V, Garcia-Saez I, Juillan-Binard C, Lantez V, Job D (2006). Microtubule regulation in mitosis, tubulin phosphorylation by the cyclin-dependent kinase Cdk1. Mol Biol Cell 17, 1041–1050.

García-Higuera I, Manchado E, Dubus P, Canamero M, Mendez J, Moreno S, Malumbres M (2008). Genomic stability and tumour suppression by the APC/C cofactor Cdh1. Nat Cell Biol 10, 802–811.

Gui L, Homer H (2012). Spindle assembly checkpoint signalling is uncoupled from chromosomal position in mouse oocytes. Development 139, 1941–1946.

Gutierrez GJ, Tsuji T, Chen M, Jiang W, Ronai ZA (2010). Interplay between Cdh1 and JNK activity during the cell cycle. Nat Cell Biol 12, 686–695.

Hached K, Xie SZ, Buffin E, Cladiere D, Rachez C, Sacras M, Sorger PK, Wassmann K (2011). Mps1 at kinetochores is essential for female mouse meiosis I. Development 138, 2261–2271.

Herbert M, Levasseur M, Homer H, Yallop K, Murdoch A, McDougall A (2003). Homologue disjunction in mouse oocytes requires proteolysis of securin and cyclin B1. Nat Cell Biol 5, 1023–1025.

Holt JE, Tran SM, Stewart JL, Minahan K, Garcia-Higuera I, Moreno S, Jones KT (2011). The APC/C activator FZR1 coordinates the timing of meiotic resumption during prophase I arrest in mammalian oocytes. Development 138, 905–913.

Homer H, Gui L, Carroll J (2009). A spindle assembly checkpoint protein functions in prophase I arrest and prometaphase progression. Science 326, 991–994.

Homer HA, McDougall A, Levasseur M, Herbert M (2005a). Restaging the spindle assembly checkpoint in female mammalian meiosis I. Cell Cycle 4, 650–653.

Homer HA, McDougall A, Levasseur M, Yallop K, Murdoch AP, Herbert M (2005b). Mad2 prevents aneuploidy and premature proteolysis of cyclin B and securin during meiosis I in mouse oocytes. Genes Dev 19, 202–207.

Howell BJ, Hoffman DB, Fang G, Murray AW, Salmon ED (2000). Visualization of Mad2 dynamics at kinetochores, along spindle fibers, and at spindle poles in living cells. J Cell Biol 150, 1233–1250.

Hunt PA, Hassold TJ (2008). Human female meiosis, what makes a good egg go bad? Trends Genet 24, 86–93.

Hwang LH, Lau LF, Smith DL, Mistrot CA, Hardwick KG, Hwang ES, Amon A, Murray AW (1998). Budding yeast Cdc20, a target of the spindle checkpoint. Science 279, 1041–1044.

Hyslop LA, Nixon VL, Levasseur M, Chapman F, Chiba K, McDougall A, Venables JP, Elliott DJ, Jones KT (2004). Ca(2+)-promoted cyclin B1 degradation in mouse oocytes requires the establishment of a metaphase arrest. Dev Biol 269, 206–219.

Jin F, Hamada M, Malureanu L, Jeganathan KB, Zhou W, Morbeck DE, van Deursen JM (2010). Cdc20 is critical for meiosis I and fertility of female mice. PLoS Genet 6, e1001147.

Jones KT (2008). Meiosis in oocytes, predisposition to aneuploidy and its increased incidence with age. Hum Reprod Update 14, 143–158.

Jones KT, Lane SI (2012). Chromosomal, metabolic, environmental, and hormonal origins of aneuploidy in mammalian oocytes. Exp Cell Res 318, 1394–1399.

Kitajima TS, Ohsugi M, Ellenberg J (2011). Complete kinetochore tracking reveals error-prone homologous chromosome biorientation in mammalian oocytes. Cell 146, 568–581.

Kolano A, Brunet S, Silk AD, Cleveland DW, Verlhac MH (2012). Error prone mammalian female meiosis from silencing the spindle assembly checkpoint without normal interkinetochore tension. Proc Natl Acad Sci USA 109, E1858–E1867.

Kudo NR *et al*. (2006). Resolution of chiasmata in oocytes requires separase-mediated proteolysis. Cell 126, 135–146.

Kuliev A, Zlatopolsky Z, Kirillova I, Spivakova J, Cieslak Janzen J (2011). Meiosis errors in over 20,000 oocytes studied in the practice of preimplantation aneuploidy testing. Reprod Biomed Online 22, 2–8.

Lane SI, Chang HY, Jennings PC, Jones KT (2011). The Aurora kinase inhibitor ZM447439 accelerates first meiosis in mouse oocytes by overriding the spindle assembly checkpoint. Reproduction 140, 521–530.

Lane SI, Yun Y, Jones KT (2012). Timing of anaphase promoting complex activation in mouse oocytes is predicted by microtubule kinetochore attachment, but not by bivalent alignment or tension. Development 139, 1947–1955.

Li M, Shin YH, Hou L, Huang X, Wei Z, Klann E, Zhang P (2008). The adaptor protein of the anaphase promoting complex Cdh1 is essential in maintaining replicative lifespan and in learning and memory. Nat Cell Biol 10, 1083–1089.

Li M, Li S, Yuan J, Wang ZB, Sun SC, Schatten H, Sun QY (2009). Bub3 is a spindle assembly checkpoint protein regulating chromosome segregation during mouse oocyte meiosis. PloS One 4, e7701.

Lister LM *et al*. (2010). Age-related meiotic segregation errors in mammalian oocytes are preceded by depletion of cohesin and Sgo2. Curr Biol 20, 1511–1521.

Listovsky T, Zor A, Laronne A, Brandeis M (2000). Cdk1 is essential for mammalian cyclosome/APC regulation. Exp Cell Res 255, 184–191.

Magidson V, O'Connell CB, Loncarek J, Paul R, Mogilner A, Khodjakov A (2011). The spatial arrangement of chromosomes during prometaphase facilitates spindle assembly. Cell 146, 555–567.

Marangos P, Verschuren EW, Chen R, Jackson PK, Carroll J (2007). Prophase I arrest and progression to metaphase I in mouse oocytes are controlled by Emi1-dependent regulation of APC(Cdh1). J Cell Biol 176, 65–75.

McGuinness BE *et al*. (2009). Regulation of APC/C activity in oocytes by a Bub1-dependent spindle assembly checkpoint. Curr Biol 19, 369–380.

Meng XQ, Fan HY, Zhong ZS, Zhang G, Li YL, Chen DY, Sun QY (2004). Localization of gamma-tubulin in mouse eggs during meiotic maturation, fertilization, and early embryonic development. J Reprod Dev 50, 97–105.

Merriman JA, Jennings PC, McLaughlin EA, Jones KT (2012). Effect of aging on superovulation efficiency, aneuploidy rates, and sister chromatid cohesion in mice aged up to 15 months. Biol Reprod 86, 49.

Michel LS, Liberal V, Chatterjee A, Kirchwegger R, Pasche B, Gerald W, Dobles M, Sorger PK, Murty VV, Benezra R (2001). MAD2 haploinsufficiency causes premature anaphase and chromosome instability in mammalian cells. Nature 409, 355–359.

Mondal G, Sengupta S, Panda CK, Gollin SM, Saunders WS, Roychoudhury S (2007). Overexpression of Cdc20 leads to impairment of the spindle assembly checkpoint and aneuploidization in oral cancer. Carcinogenesis 28, 81–92.
Nagaoka SI, Hodges CA, Albertini DF, Hunt PA (2011). Oocyte-specific differences in cell-cycle control create an innate susceptibility to meiotic errors. Curr Biol 21, 651–657.
Ookata K, Hisanaga S, Bulinski JC, Murofushi H, Aizawa H, Itoh TJ, Hotani H, Okumura E, Tachibana K, Kishimoto T (1995). Cyclin B interaction with microtubule-associated protein 4 (MAP4) targets p34cdc2 kinase to microtubules and is a potential regulator of M-phase microtubule dynamics. J Cell Biol 128, 849–862.
Perera D, Tilston V, Hopwood JA, Barchi M, Boot-Handford RP, Taylor SS (2007). Bub1 maintains centromeric cohesion by activation of the spindle checkpoint. Dev Cell 13, 566–579.
Peters JM (2006). The anaphase promoting complex/cyclosome: a machine designed to destroy. Nat Rev Mol Cell Biol 7, 644–656.
Pfleger CM, Kirschner MW (2000). The KEN box, an APC recognition signal distinct from the D box targeted by Cdh1. Genes Dev 14, 655–665.
Potapova TA, Daum JR, Pittman BD, Hudson JR, Jones TN, Satinover DL, Stukenberg PT, Gorbsky GJ (2006). The reversibility of mitotic exit in vertebrate cells. Nature 440, 954–958.
Qiao X, Zhang L, Gamper AM, Fujita T, Wan Y (2010). APC/C-Cdh1: from cell cycle to cellular differentiation and genomic integrity. Cell Cycle 9, 3904–3912.
Reis A, Levasseur M, Chang HY, Elliott DJ, Jones KT (2006). The CRY box: a second APC cdh1-dependent degron in mammalian cdc20. EMBO Rep 7, 1040–1045.
Reis A, Madgwick S, Chang HY, Nabti I, Levasseur M, Jones KT (2007). Prometaphase APC cdh1 activity prevents non-disjunction in mammalian oocytes. Nat Cell Biol 9, 1192–1198.
Schindler K, Schultz RM (2009). CDC14B acts through FZR1 (CDH1) to prevent meiotic maturation of mouse oocytes. Biol Reprod 80, 795–803.
Solc P, Schultz RM, Motlik J (2010). Prophase I arrest and progression to metaphase I in mouse oocytes: comparison of resumption of meiosis and recovery from G2-arrest in somatic cells. Mol Hum Reprod 16, 654–664.
Song L, Rape M (2010). Regulated degradation of spindle assembly factors by the anaphase promoting complex. Mol Cell 38, 369–382.
Verlhac MH, Terret ME, Pintard L (2010). Control of the oocyte-to-embryo transition by the ubiquitin-proteolytic system in mouse and *C. elegans*. Curr Opin Cell Biol 22, 758–763.
Wasch R, Robbins JA, Cross FR (2010). The emerging role of APC/CCdh1 in controlling differentiation, genomic stability and tumor suppression. Oncogene 29, 1–10.
Wassmann K, Niault T, Maro B (2003). Metaphase I arrest upon activation of the Mad2-dependent spindle checkpoint in mouse oocytes. Curr Biol 13, 1596–1608.
Yamamuro T, Kano K, Naito K (2008). Functions of FZR1 and CDC20, activators of the anaphase-promoting complex, during meiotic maturation of swine oocytes. Biol Reprod 79, 1202–1209.
Zachariae W, Schwab M, Nasmyth K, Seufert W (1998). Control of cyclin ubiquitination by CDK-regulated binding of Hct1 to the anaphase promoting complex. Science 282, 1721–1724.
Zhang D, Yin S, Jiang MX, Ma W, Hou Y, Liang CG, Yu LZ, Wang WH, Sun QY (2007). Cytoplasmic dynein participates in meiotic checkpoint inactivation in mouse oocytes by transporting cytoplasmic mitotic arrest-deficient (Mad) proteins from kinetochores to spindle poles. Reproduction 133, 685–956.
Zur A, Brandeis M (2002). Timing of APC/C substrate degradation is determined by fzy/fzr specificity of destruction boxes. EMBO J 21, 4500–4510.